Postharvest Biology and Technology 67 (2012) 37–43

Contents lists available at SciVerse ScienceDirect

Postharvest Biology and Technology

journal homepage: www.elsevier.com/locate/postharvbio

# Measurement and evaluation of tomato maturity using magnetic resonance imaging

Lu Zhang [a], Michael J. McCarthy [a,b,*]

[a] Department of Food Science and Technology, University of California, Davis One Shields Avenue, Davis, CA 95616, United States
[b] Department of Biological and Agricultural Engineering, University of California, Davis One Shields Avenue, Davis, CA 95616, United States

ARTICLE INFO

*Article history:*
Received 20 June 2011
Accepted 9 December 2011

*Keywords:*
Tomato
Maturity
Magnetic Resonance imaging (MRI), PLS-DA
$T_2$
Diffusion rate

ABSTRACT

Tomato maturity is one of the most important factors associated with the quality of processed tomato products. Magnetic resonance imaging (MRI) is capable of probing the local environment and density of water protons, and encoding the differences in water properties in the form of contrast in image signal intensity. This study investigated changes in tomatoes at different maturity using MRI and the potential for using MRI for tomato maturity classification. A set of 5 MR images was collected on processing tomatoes at various maturity stages. The 5 MRI sequences were selected so that information on water proton properties, including proton density, $T_1$, $T_2$, and diffusion rate, are encoded in the MR image signal intensity. A relative water diffusion rate map was also calculated. Changes in structural features and volume element (voxel) intensity in the images were observed as tomatoes develop from green to red stage. In image analysis, voxels in the region of interest (ROI) corresponding to the pericarp of the tomato were used to calculate statistical features of the voxel intensity for image characterization. Partial least square discriminant analysis (PLS-DA) was applied to a total of 48 image features calculated from 5 MR images of 144 processing tomatoes to predict the tomato maturity. The model with 4 latent variables captures 70% of the variation in tomato maturity. The classification accuracies of the PLS-DA model were around 90% for green, breaker-light red, and red maturity stages. The Variable Importance in Projection coefficient of the 48 image features in the model indicated that the diffusion weighted image and spin echo image with higher $T_2$ weighting were most important for tomato maturity classification.



## 1. Introduction

Different tomato products have distinct requirements for maturity to achieve quality standards; hence, tomato maturity is one of the most important factors associated with the quality of processed tomato products. During ripening, tomato fruit go through a series of highly ordered physiological and biochemical changes. Biochemical changes, such as increased respiration, chlorophyll degradation, biosynthesis of carotenoids, starch degradation, and increased activity of cell wall-degrading enzymes, bring on changes in color, firmness, and development of aromas and flavors (Prasanna et al., 2007). Tomato maturity has been related to quantifiable parameters, which reflect the biochemical changes during ripening. Color is used as a major method in determining maturity of tomato. However, skin color of tomato varies from cultivar to cultivar even at the same maturity stage (Molyneux et al., 2004). In tomato processing, the fruit fed to the processing line are often a mixture of tomatoes of multiple cultivars, in which case color may not be a reliable indicator for maturity.

Tomato ripening is associated with a number of variations in chemical composition, cellular structure, and internal structure of the fruit. The concentration in reducing sugars and carotenes increases, whereas those in titratable acidity, chlorophylls, and chlorogenic acid content decreases (Gautier et al., 2008). Degradation of the cell wall polysaccharides induces fruit softening (Gross and Wallner, 1979). It is difficult to find a quality attribute to characterize the intricate process of ripening. Ideally a technique which can measure either compositional changes or structural changes noninvasively and nondestructively may provide a method to more accurately characterize ripening.

Magnetic resonance imaging (MRI) is a nondestructive imaging technique which uses the magnetic properties of nuclei and their interactions with radio frequency and applied magnetic fields. Water proton relaxation behavior is sensitive to the local environment of water and the material structure, thus water proton relaxation times are a measure of a combination of many factors. Variations in chemical compounds and cellular structure lead to change in water proton relaxation times, which will change

* Corresponding author at: Department of Food Science and Technology, University of California, Davis, One Shields Avenue, Davis, CA 95616, United States.
Tel.: +1 530 752 8921; fax: +1 530 752 4759.
*E-mail address:* mjmccarthy@ucdavis.edu (M.J. McCarthy).

0925-5214/$ – see front matter © 2011 Elsevier B.V. All rights reserved.
doi:10.1016/j.postharvbio.2011.12.004

**Table 1**
MRI pulse sequence parameters.

| Pulse sequence | TE (ms) | TR (ms) | FOV (mm × mm) | Slice thickness (mm) |
|---|---|---|---|---|
| SE 1 | 60 | 200 | 70 × 70 | 8 |
| SE 2 | 6.9 | 100 | 70 × 70 | 8 |
| SE 3 | 6.9 | 600 | 70 × 70 | 8 |
| DW SE 1 | 38 | 268 | 95 × 95 | 5 |
| DW SE 2 | 38 | 268 | 95 × 95 | 5 |

the signal in MR images. MRI provides an opportunity to observe changes both in the local water proton environment and the structure in fruit. In the study of tomato fruit, MRI was first used by Ishida et al. (1989) and they found that MRI is able to distinguish the physiological variations among different types of tissues and the physiological changes during ripening of tomato fruit. Saltveit (1991) demonstrated that the difference in tomato fruit at different mature green stages can be visualized in MR images. The change in macroscopic structure and water proton relaxation times during ripening of tomato fruit have been investigated by Musse et al. (2009a). Although limited quantity of sample was used in the study, modification in outer pericarp structure followed a different pattern during ripening of tomato than other internal tissues. Thus, biological variation between individual fruit may interfere with the success of correlations based on relaxation time measurements that average contributions from the entire fruit when attempting to characterize the variation in tomatoes at different maturity stages. This type of behavior was observed by Tu et al. (2007), when using whole fruit spin–spin relaxation time values of many fruit over several seasons to correlate to quality.

The objectives of this study were to investigate the physiological changes of tomato at different maturity stages discernible in MR images, and to develop an effective multivariate model to classify tomatoes at different maturity stages. A large sample size was used to determine if natural biological variance would mask changes in MRI data associated with changes in tomato maturity.

## 2. Materials and methods

### 2.1. Sample selection

Processing tomatoes, cvs. AB 5210, were provided by ConAgra Foods (Oakdale, CA). The tomatoes were harvested from the field at different maturity stages and spanning the range of 6 stages, i.e., green, breaker, turning, pink, light red, and red based on their surface color. The tomato fruit were hand washed and sorted into three classes: green, breaker-light red (breaker, turning, pink, and light red), and red. A total of 144 defect-free tomato fruit were used in the study, using approximately equal amounts fruit for each class. Samples were equilibrated to room temperature (22 °C) prior to analysis.

### 2.2. MRI acquisition

MRI data was acquired on a 1 T permanent magnet MRI system (Aspect AI, Industrial Area Hevel Modi'in, Shoham, Israel) with a 60 × 90 cm elliptical RF coil at 22 °C. Tomatoes were placed on a plastic sample holder and manually centered so that the stem-blossom-end axis of fruit aligned with the center of the coil. The image of the longitude slice along the stem-blossom-end axis of each tomato was acquired. A set of 5 MR images was collected for each sample with different sequences. The 5 MRI sequences were selected so that information on water proton properties, including proton density, relaxation times, and diffusion rate, are embedded in the MR image intensity (Table 1). In spin echo images, the signal intensity is modeled by Bernstein et al. (2004):

$$S = M_0(1 - 2e^{-(\mathrm{TR}-\mathrm{TE})/T_1} + e^{-\mathrm{TR}/T_1})e^{-\mathrm{TE}/T_2} \quad (1)$$

where $M_0$ is the net magnetization, being directly proportional to the water proton density, $T_1$ is the spin–lattice relaxation time, and $T_2$ is the spin–spin relaxation time. Repetition time (TR) and Echo time (TE) are sequence parameters setting the interval between pulses. At a given TR and TE, the signal intensity of each voxel is determined by the characteristic $M_0$, $T_1$, and $T_2$ of the material in the voxel. The TE and TR of spin echo sequence (SE) were adjusted to obtain $T_1$ and/or $T_2$ intensity weighted images. Diffusion weighted imaging was used to acquire information on the changes in water diffusion coefficient. In diffusion weighted imaging (DW SE2), a pair of gradient pulse, with $\delta$ = 10.2 ms, $\Delta$ = 23.938 ms, and $G$ = 0.0804 T/m, were added to a spin echo sequence. Movement of water molecules within the time between the two pulses results in signal intensity attenuation. DW SE 1 is a spin echo sequence with all parameters the same as DW SE 2, except that no gradient pulse was applied. The signal attenuation caused by the pulse gradient is determined by the apparent diffusion coefficient of water. A diffusion coefficient weighted intensity image was obtained by taking the ratio of DW SE2 to DW SE1 voxel by voxel (Fig. 1).

### 2.3. Data analysis

Variation in chemical composition and macrostructure of tomato tissue led to differences in water proton relaxation times and contrast in MR images (Musse et al., 2009b). In addition, changes in the relaxation times depended on tissue type during ripening (Musse et al., 2009a). However, open cavities were observed between the locular gel and pericarp in some samples. Therefore, quantitative image analysis was performed only on pericarp to avoid the interference of the open cavity in locular tissue. A region of interest (ROI) corresponding to the tissue of interest (pericarp) was defined for images of each sample (Fig. 2).

For each of the MR images, mean and histogram features (median, mode, variance, skewness, kurtosis, range, and contrast) of the voxel intensities in the ROI were calculated. Partial least square discriminant analysis (PLS-DA) was performed using the calculated image features as $x$ variables (48 variables) and three maturity classes (green, breaker-light red, red) as $y$ variables to deduce a maturity classification model. Matlab release 2010a (The mathworks, Natick, MA) and PLS_toolbox (Eigenvector Research Inc., Wenatchee, WA) were used for model development. In PLS-DA, latent variables, which are the linear combinations of $x$ variables, were computed to maximize the explanation of variance in $x$ variables and $y$ variables. PLS-DA algorithm attempts to discriminate each individual class from the rest. To achieve binary classification of three tomato maturity classes from each other, the PLS-DA model calculated a set of three regression vectors, one for each class. Cross-validation was performed to evaluate the predictive ability of the model.

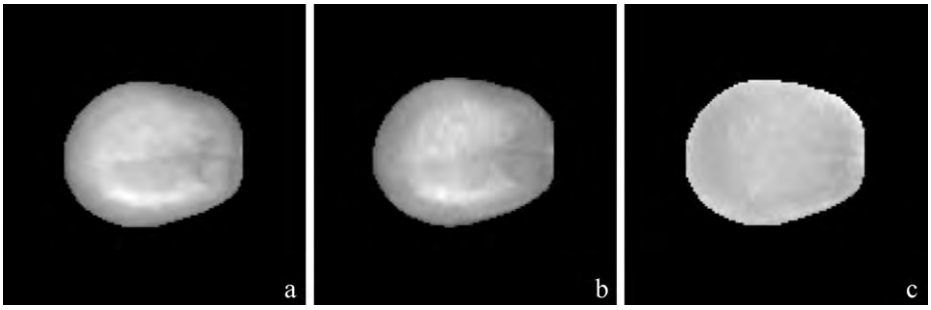


**Fig. 1.** An example of diffusion rate image (c) obtained by division of DW SE2 (b) image by DW SE1 image (a) of the same tomato.

## 3. Results and discussion

### 3.1. MR image analysis

Displayed in Fig. 3 were the typical images for tomatoes of the three maturity categories. For each image type the voxel intensity pattern varies as a function of maturity, as a result of biological variability and the impact of these on the intrinsic NMR properties of the protons. For each tomato at a specific maturity stage the voxel intensity pattern within the tomato for each image type is different. The anatomical features of the tomato were best captured in the image type SE1 (Fig. 3) for all maturity stages. Pericarp layers, locular tissues, and placenta were visible in SE1. As tomatoes developed from green to red stage, the contrast between different tissues changed (Fig. 3). Quantitative comparison of the data was based on extracting voxel intensity values from the images.

Mean voxel intensities in the pericarp region of images were summarized in Table 2. As shown in Eq. (1), the images, acquired with various combinations of TR and TE, have different contrast emphasizing different water proton properties. SE2, with short TR and TE, is a $T_1$ weighted image. In SE1, more $T_2$ weighting was introduced by using a longer TE compared to SE2. The mean voxel intensity in SE2 images of "breaker-light red" tomatoes decreased considerably compared to "green" fruit. The tomatoes at "red" stage had a mean voxel value of SE2 image comparable to "green" tomatoes. Therefore, the averaged $T_1$ relaxation time of pericarp increased at "breaker-light red" stage and then decreased to similar level to "green" fruit at "red" stage. The mean voxel intensity in SE1 of fruit at "breaker-light red" stage was smaller than "green" stage tomatoes, and there is no significant difference between the SE1 mean voxel intensity of "red" and "breaker-red" tomatoes. The contrast in SE1 image was based on $T_1$ and $T_2$ weighting. The divergence between the change in mean voxel intensity of SE2 and SE1 was primarily a result of the greater $T_2$ weighting, as well as less $T_1$ weighting, in SE1. The decreased intensity of SE2 at "breaker-red" and red stage might be caused by shorter $T_2$ relaxation time in pericarp, which exceeded the changes in $T_1$ relaxation time. Similar change in $T_2$ value was observed in $T_2$ relaxation time measurement of tomato pericarp at the three maturity stages (results not shown).

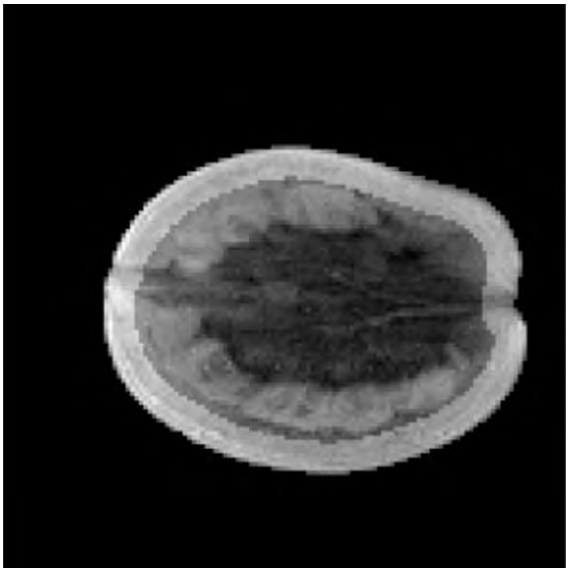

**Fig. 2.** ROI (high lighted) mask overlaid on a tomato spin echo image.

Although the contrast in five images was unalike, the variation pattern in mean intensity of SE3, DW SE1, and DW SE2 were similar to SE2. The mean value of DW SE2/DW SE1 in tomato pericarp decreased from 0.55 for tomatoes at "green" stage to 0.36 for tomatoes at "red" stage, indicating that the water diffusion coefficient of tomato pericarp gradually increased during ripening. In plant tissue like tomato, the presence of cell membrane may impede the movement of water molecules. A barrier that restricts the diffusion of water results in a smaller apparent diffusion coefficient. It is likely that the measured water apparent diffusion rate is affected by the size of the vacuole and the cell. In a time frame that is long enough for the water molecule to reach the barrier, the apparent diffusion coefficient of water would be greater in big cells than in small cells. In the diffusion weighted sequence, the probed water diffusion displacement was around 10 μm during the measurement. Possible boundary effect may be reflected in the measured water diffusion rate. The increase in the apparent diffusion rate of water may be ascribed to an increase in the cell size during ripening. At the same time, cell membranes are permeable boundaries. An increase in the cell membrane permeability would somewhat alleviate the restriction from the barrier. On the other hand, water in each cell compartment has a different diffusion coefficient. Duval et al. (2005) detected three diffusion components in tomato pericarp cell, corresponding to cell wall-extracellular space, cytoplasm, and vacuole. During ripening, water redistribution among the three compartments may contribute to the change in water diffusion coefficient. In addition, development of gas bubble content in tomato pericarp during ripening was reported in several studies (Saltveit, 1991; Musse et al., 2009a). Such occurrence of air in the tissue would increase the internal magnetic field gradients. Greater internal magnetic field gradients in the tomato effectively increase the decay by adding to the applied gradient (Hills, 2006), resulting in an increase in apparent water diffusion coefficient.

Variance of voxel intensity of each image type was also calculated to obtain the variability of voxel intensity. As shown in Table 3, fruit at "breaker-light red" stage had the least variability in all image types except for DW SE2/DW SE1. The variance of SE1, SE3, DW SE1, and DW SE2 demonstrated similar pattern of change at different maturity stage. In those images, tomatoes at "green" stage had the highest variance, followed by tomatoes at "red" stage. For the

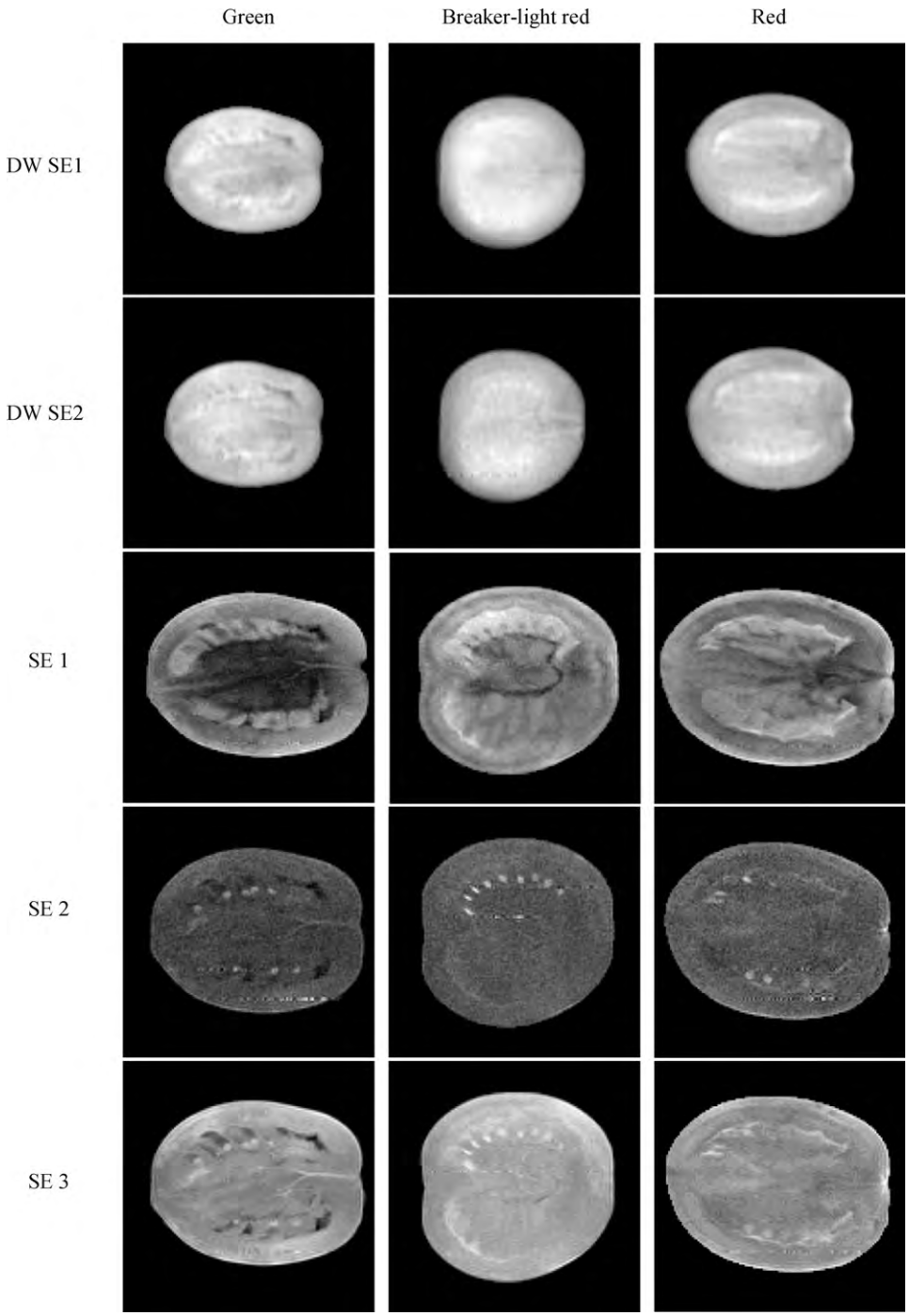


**Fig. 3.** Example of MR images of tomatoes at three maturity stages.

variance in SE2 image, "Red" stage tomatoes showed the highest value. The variances in DW SE2/DW SE1 of three maturity stages were not significantly different from each other. The variance of voxel intensity in MR images generally gave information on variability of water proton properties in tomato pericarp. Thus, the variation of water relaxation time within tomato pericarp was the smallest at "breaker" stage. Tomatoes at "red" stage varied most in terms of $T_1$ relaxation time.

**Table 2**
Mean voxel intensity in ROI of MR images of tomato at different maturity stage.*

| | SE 1 (AU) | SE 2 (AU) | SE 3 (AU) | DW SE1 (AU) | DW SE2 (AU) | DW SE2/DW SE1 (AU) |
|---|---|---|---|---|---|---|
| Green | 1852[a] | 659[a] | 1366[a] | 64119[a] | 21672[a] | 0.55[a] |
| Breaker-light red | 1522[b] | 557[b] | 1228[b] | 58905[b] | 19113[b] | 0.41[b] |
| Red | 1563[b] | 679[a] | 1394[a] | 70645[c] | 21890[a] | 0.36[c] |

* Values with the same letters in the same column are not significantly different at $P = .05$.

**Table 3**
Variance of voxel intensity in ROI of MR images of tomato at different maturity stage.*

| | SE 1 ($\times 10^5$ AU$^2$) | SE 2 ($\times 10^4$ AU$^2$) | SE 3 ($\times 10^4$ AU$^2$) | DW SE1 ($\times 10^8$ AU$^2$) | DW SE2 ($\times 10^7$ AU$^2$) | DW SE2/DW SE1 (AU$^2$) |
|---|---|---|---|---|---|---|
| Green | 1.31[a] | 2.06[a] | 4.84[a] | 1.77[a] | 2.21[a] | 0.72[a] |
| Breaker-light red | 0.774[b] | 1.38[b] | 3.87[b] | 1.27[b] | 1.32[b] | 1.23[a] |
| Red | 0.973[c] | 2.59[c] | 4.37[a,b] | 1.40[b] | 1.56[b] | 0.38[a] |

* Values with the same letters in the same column are not significantly different at $P = .05$.

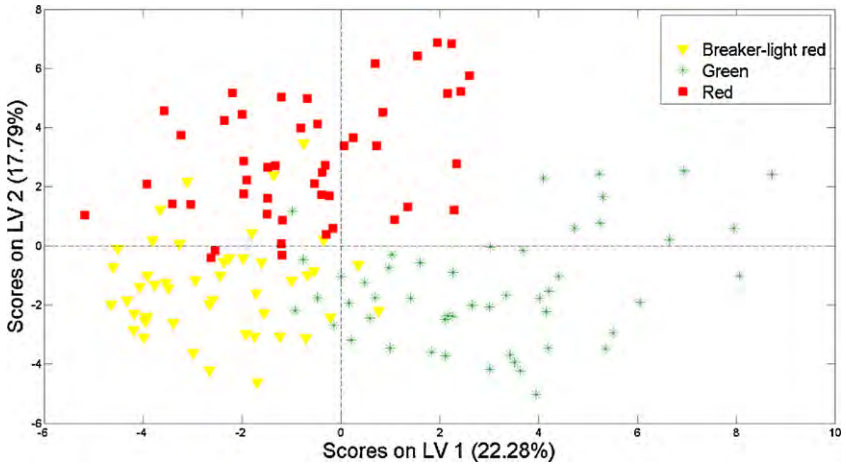


**Fig. 4.** PLS–DA score plot of tomato samples.

### 3.2. PLS-DA model for maturity classification

Although mean and variance of signal intensity in images provided useful data for differentiation of tomato at different maturity, additional images features were calculated to capture more information from an image. Discriminant analysis was performed using PLS-DA on the images features to determine whether it was possible to distinguish tomatoes at different maturity on the basis of MR images. Cross-validation was performed by random splitting the dataset in half. One subset was used as training data to develop a model, and the other subset was applied to test the model performance. The random subset cross-validation was repeated 20 times. The root mean square error of cross validation (RMSECV) value was a function of number of latent variables in the model. A PLS-DA model with 4 latent variables was generated based on the criteria of minimizing RMSECV with the least number of latent variables. The 4-latent-variable model captured 48% of the variance in x (image features of ROI in the MR images) and 70% of the variance in y (maturity). The PLS-DA score plot of the first two latent variables showed clustering of tomato samples at the same maturity stage (Fig. 4). Although within-class variation is notable, the between-class variation is more significant.

The correlation coefficient of cross-validation ($r_{cv}$) for "green", "breaker-light red", and "red" stages were 0.842, 0.746, and 0.796, respectively. Table 4 shows more model performance parameters of the PLS-DA model, including root mean square error of calibration (RMSEC), RMSECV, sensitivity and specificity. RMSECV is a measure of a model's ability to predict new samples that were not used to build the model (Mclennan, 1995). RMSECVs were very close to RMSECs, which means the loss in the accuracy was very small when the calibration models were applied to new samples. Sensitivity (percent of true positive) and specificity (percent of true negative) evaluate the accuracy of the classification model. The PLS-DA model for all three maturity stages had sensitivity and specificities of around 90%. All the above parameters demonstrated that the PLS-DA model is fairly robust for prediction of the three tomato maturity stages.

**Table 4**
Model performance parameter of PLS-DA model.

| | Green | Breaker-light red | Red |
|---|---|---|---|
| RMSEC | 0.234 | 0.287 | 0.255 |
| RMSECV | 0.275 | 0.335 | 0.302 |
| Sensitivity | 0.919 | 0.885 | 0.907 |
| Specificity | 0.946 | 0.886 | 0.907 |

Variable Importance in Projection (VIP) coefficient reflects the importance of each $x$ variable in the prediction model. In other words, the image types and features that most strongly influence separation of different tomato maturity stages were indicated by the VIP coefficients (Fig. 5). $X$ variables with a large VIP, larger than one, are most influential for the model (Eriksson et al., 2006). Because each maturity class had its own set of regression vectors, the VIP coefficients for "green", "breaker-light red", and "red" classification were different. The most important image features responsible for prediction of "green" were mainly image features, such as mean, variance, skewness, kurtosis, and range, of image SE1, DW SE2/DW SE 1, DW SE2, and DW SE1 (Fig. 5a). For discrimination of "break-light red", several features of DW SE1, DW SE2, DW SE2/DW SE1 and SE1 had a significant contribution. Voxel intensity mean, median, mode, and kurtosis of SE3 were slightly above one (Fig. 5b). The DW SE1, DW SE2/DW SE1, DW SE2, and SE1 statistical features were the major variables responsible for the classification of "red" stage tomatoes (Fig. 5c). Some quantitative values of SE2 and SE3 also had VIP coefficients a little greater than one. Therefore, the top image types for classification of "green", "breaker-light red", and "red" tomatoes were DW SE1, DW SE2, SE1, and DW SE2/DW SE1. Image statistical features of these images, especially median, mean, variance, kurtosis, and range had considerable contribution to the PLS-DA predictive model.

Considering the contrast in MR images, the importance of each image type for tomato maturity classification represents the contribution of corresponding water proton properties. All image types had a different combination of proton density, $T_1$ and $T_2$ relaxation time weighting. There was greater $T_2$ weighting in DW SE 1, DW SE 2, and SE1 than SE2 and SE3. SE 1 had the highest $T_2$

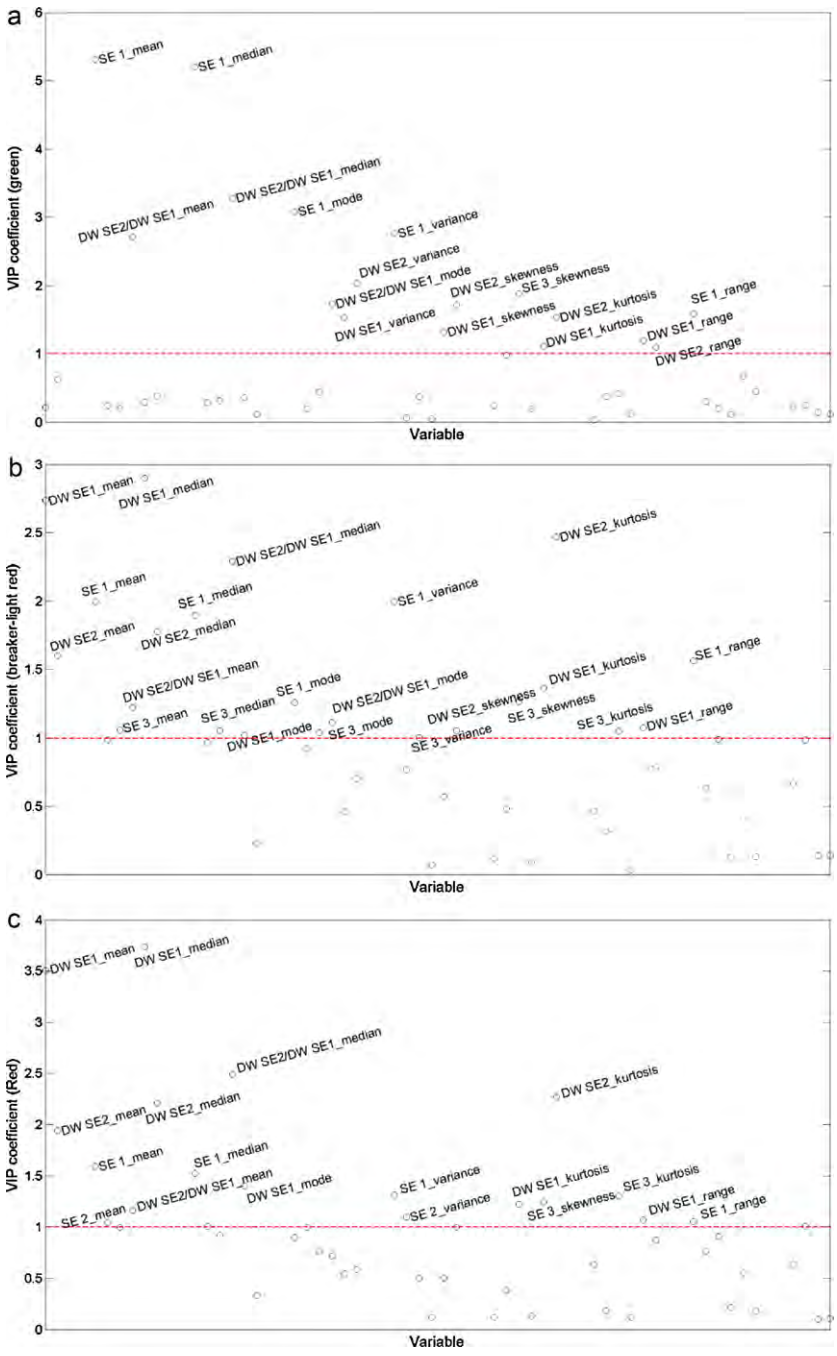


**Fig. 5.** VIP coefficients of *x* variables for each maturity class prediction model: (a) green, (b) breaker-light red, (c) red.

weighting among all the images. It is plausible that $T_2$ relaxation time of the pericarp region was an essential factor relating to tomato maturity. The importance of the DW SE2 and DW SE2/DW SE1 demonstrated that the apparent water diffusion rate was a main indicator of tomato maturity change as well. Although the apparent diffusion rate of water acquired using the diffusion weighted sequence was not the "real" water self-diffusion rate, it was a measure of coactions of important physiological changes, including cell size, membrane permeability, air cavity development, and water diffusion rate. In addition to the averaged water proton properties of the tomato pericarp tissue, the variability and distribution of water proton properties in the tissue also contributed to the differentiation of maturity stages.

## 4. Conclusions

Physiological changes in tomato at different maturity stages can be encoded in MR image signal intensity. The large sample size in this study made it possible to include natural biological variation into the prediction model. Since the data analysis was only performed on ROI of images corresponding to tomato pericarp tissue, the change in pericarp tissue offered enough information for tomato maturity differentiation. Besides the mean voxel intensity of MR images, variation and distribution of voxel intensity in image were important factors in tomato maturity classification. PLS-DA modeling of MR images provided an effective method for predicting tomato maturity.

## Acknowledgements

This work was partially supported by ConAgra Foods, Inc. and by National Research Initiative Award 2007-02632 from the USDA National Institute of Food and Agriculture.

## References

Bernstein, M., King, K., Zhou, X., 2004. Handbook of MRI Pulse Sequences. Academic Press.

Duval, F., Cambert, M., Mariette, F., 2005. NMR study of tomato pericarp tissue by spin-spin relaxation and water self-diffusion. Applied Magnetic Resonance 28, 29–40.

Gautier, H., Diakou-Verdin, V., Bénard, C., Reich, M., Buret, M., Bourgaud, F., Poëssel, J.L., Caris-Veyrat, C., Génard, M., 2008. How does tomato quality (sugar, acid, and nutritional quality) vary with ripening stage, temperature, and irradiance? Journal of Agricultural and Food Chemistry 56, 1241–1250.

Gross, K.C., Wallner, S.J., 1979. Degradation of cell wall polysaccharides during tomato fruit ripening. Plant Physiology 63, 117–120.

Hills, B.P., 2006. NMR relaxation and diffusion studies of horticultural products. In: Webb, G.A. (Ed.), Modern Magnetic Resonance. Springer, Netherlands, pp. 1721–1727.

Ishida, N., Kobayashi, T., Koizumi, M., Kano, H., 1989. H-1-NMR imaging of tomato fruits. Agricultural and Biological Chemistry 53, 2363–2367.

Eriksson, L.E.J., Kettaneh-Wold, N., Wold, S., 2006. Multivariate and Megavariate Data Analysis Basic Principles and Applications. Umetrics AB, Umea, Sweden.

Mclennan, F.a.B.K., 1995. Process Analytical Chemistry. Blackie Academic & Professional, London.

Molyneux, S.L., Lister, C.E., Savage, G.P., 2004. An investigation of the antioxidant properties and colour of glasshouse grown tomatoes. International Journal of Food Sciences and Nutrition 55, 537–545.

Musse, M., Quellec, S., Cambert, M., Devaux, M.F., Lahaye, M., Mariette, F., 2009a. Monitoring the postharvest ripening of tomato fruit using quantitative MRI and NMR relaxometry. Postharvest Biology and Technology 53, 22–35.

Musse, M., Quellec, S., Devaux, M.F., Cambert, M., Lahaye, M., Mariette, F., 2009b. An investigation of the structural aspects of the tomato fruit by means of quantitative nuclear magnetic resonance imaging. Magnetic Resonance Imaging 27, 709–719.

Prasanna, V., Prabha, T.N., Tharanathan, R.N., 2007. Fruit Ripening Phenomena – An Overview, Critical Reviews in Food Science & Nutrition. Taylor & Francis Ltd, pp. 1–19.

Saltveit Jr., M.E., 1991. Determining tomato fruit maturity with nondestructive in vivo nuclear magnetic resonance imaging. Postharvest Biology and Technology 1, 153–159.

Tu, S.S., Choi, Y.J., McCarthy, M.J., McCarthy, K.L., 2007. Tomato quality evaluation by peak force and NMR spin–spin relaxation time. Postharvest Biology and Technology 44, 157–164.